A sequential approach to resonant magnetotunnelling in double-barrier heterostructures

1994 J. Phys.: Condens. Matter 6 10031

(http://iopscience.iop.org/0953-8984/6/46/020)

J. Phys.: Condens. Matter 6 (1994) 10031–10042. Printed in the UK

A sequential approach to resonant magnetotunnelling in double-barrier heterostructures

Xue-Hua Wang†‡, Jian-Ping Peng†§, Tong-Zhong Li†, Shi-Wei Gu†, W S Li‖ and Y Y Yeung¶

† Institute of Condensed Matter Physics, Shanghai Jiao Tong University, Shanghai 200030, People's Republic of China

‡ Physics Department, Xiang Tan University, Xiang Tan, Hunan 411105, People's Republic of China

§ China Centre of Advanced Science and Technology (World Laboratory), PO Box 8730, Beijing 100080, People's Republic of China

‖ Electronic Engineering Department, Hong Kong Polytechnic, Hunghom, Hong Kong

¶ Applied Physics Department, Hong Kong Polytechnic, Hunghom, Hong Kong

Received 24 January 1994, in final form 11 May 1994

Abstract. We study the resonant tunnelling in double-barrier heterostructures via Landau levels in the sequential tunnelling approach. The effects of the space-charge formation in the electrodes and in the well together with inelastic-scattering broadening are taken into account. Under appropriate approximations, the tunnelling current and differential conductance can be written as simpler forms which analytically reproduce the main features of experiments. Then the dependences on the temperature and magnetic field are studied numerically; these are also in accordance with experiments.

1. Introduction

Since the pioneering work of Tsu and Esaki [1, 2] on resonant tunnelling in quantum-well structures, double-barrier heterostructures (DBHSs) have attracted a great deal of attention [3–6] owing to the relative ease of fabrication and many interesting features such as negative differential conductance (NDC) [7, 8], fast response time [9] and intrinsic bistability [10–14]. Because of these new features, the DBHSs have potentiality for many practical applications. There are mainly two theoretical pictures in studies of the resonant tunnelling in the DBHSs. The first one is the global tunnelling model (GTM) [3, 15, 16], in which the incident electron is characterized by a plane wave with a well defined energy. By use of the transfer-matrix technique, the total transmissivity of the structure is determined as a function of the incident electron energy and an applied bias perpendicular to the interfaces. The tunnelling current of the system is obtained from the total transmission coefficient of the whole structure. The second picture is the sequential tunnelling model (STM) proposed by Luryi [7]. In this theoretical picture [17, 18, 11, 12], the resonant tunnelling in the DBHSs is regarded as two successive processes, in which the three-dimensional (3D) state electrons in the emitter tunnel into the two-dimensional (2D) quasibound states in the well and subsequently escape from the well into 3D states in the collector. According to this model, the resonant tunnelling occurs when the longitudinal energy ε_z of the incident electron coincides with the quasibound level in the well determined by the one-dimensional potential, and stops suddenly when the quasibound level in the well is just below the bottom of the conduction

0953-8984/94/4610031+12$19.50

band of the emitter since the component of the electron momentum parallel to the interfaces as well as the electron energy is conserved. It has been shown that the two interpretations are equivalent and lead to the same predictions for the DC current when no magnetic field is applied and inelastic-scattering processes are not included [18].

Recently there has been intensive attention paid to the resonant magnetotunnelling in DBHSs because it has been proved to be a powerful tool to study the dynamics of electrons in them [19–25]. In research on resonant tunnelling in DBHSs when a magnetic field is applied perpendicular to the growth direction, the GTM has been used theoretically to study the magnetotunnelling current and intrinsic bistability without considering inelastic-scattering processes [21, 22]. The effect of the magnetic field is considered by introducing an effective potential $V_n(z) = \hbar\omega_c(z)(n + \frac{1}{2}) + V(z)$, where $\omega_c(z)$ is the cyclotron frequency and $V(z)$ is the one-dimensional potential for zero magnetic field. Then the current is determined through calculation of the total elastic transmission coefficient T_e of the structure. The numerical results are found to be in agreement with experiments in describing the main features. Schulz and Tejedor [26] developed the GTM to study resonant magnetotunnelling processes associated with inelastic events by adding the inelastic contribution term $(\Gamma_i/\Gamma_e)T_e$ to the total transmission coefficient (where Γ_i and Γ_e are respectively inelastic and elastic scattering half-widths). Their calculations have improved the overall shape of the current density curves. But there are still considerable quantitative discrepancies between experiments and their theoretical calculations in predicting the peak position of the curves and the position of the negative differential conductance. Note that the earlier experiments were interpreted in terms of the sequential tunnelling model [19, 20] and Platero *et al* [27] have applied it to study DBHSs with an applied magnetic field perpendicular to the current. Although the physics has been described by these authors, it is worthwhile to study it theoretically in more detail. Moreover the STM provides a natural frame in which the effects of the space-charge accumulation in the electrodes and in the well may be conveniently considered. Hence, we present here results of the resonant tunnelling via Landau levels in DBHSs with an applied magnetic field parallel to the current in the STM. Expressions for the tunnelling current and differential conductance are derived on a firm background. Under appropriate approximations, it is then shown that the tunnelling current and differential conductance can be written as simpler forms which analytically reproduce the main features of experiments. The results here will show that the space-charge formation in the electrodes and in the well plays an important role in determining the overall shape of the current density and differential conductance curves as well as their peak positions. Finally, the dependences on the temperature and magnetic field are studied numerically.

2. Theory and calculations

We consider a DBHS consisting of n^+-GaAs (emitter)/$Ga_{(1-x)}Al_xAs$ (first barrier)/GaAs (well)/$Ga_{1-x}AlAs$ (second barrier)/n^+-GaAs (collector). A magnetic field B and a bias of voltage v are applied perpendicular to the interfaces. Our analysis is restricted to the conduction-band bottom of the structure with the standard effective-mass parabolic-band approximation. Firstly, we ignore the effects of the space-charge in the electrodes and in the well. The potential diagram of a DBHS with an applied bias is shown in figure 1(*b*). To avoid unnecessary numerical complications, we replace the actual potential (solid line in figure 1(*b*)) by a simpler step potential (dotted line in figure 1(*b*)). The errors thus introduced are generally believed to be too small to affect the quantitative results when the

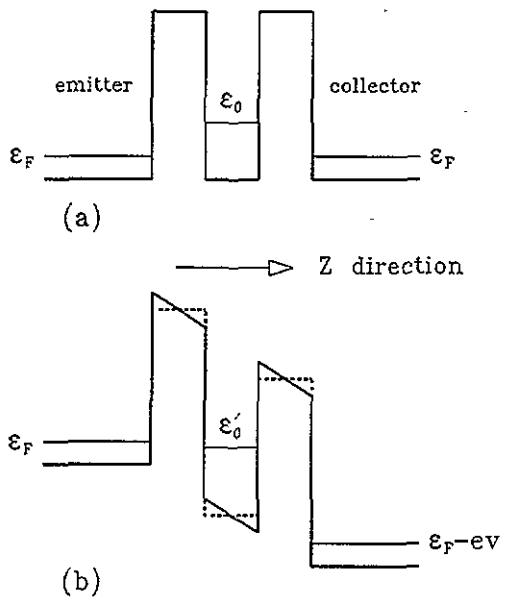

Figure 1. Conduction-band diagram of a double-barrier heterostructure, sandwiched between an emitter (n^+-GaAs) and a collector (n^+-GaAs). ε_F is the Fermi energy level in the electrodes. ε_0 and ε_0' correspond to the longitudinal quasibound levels in the well. (*a*) Without an applied voltage. (*b*) With an applied voltage.

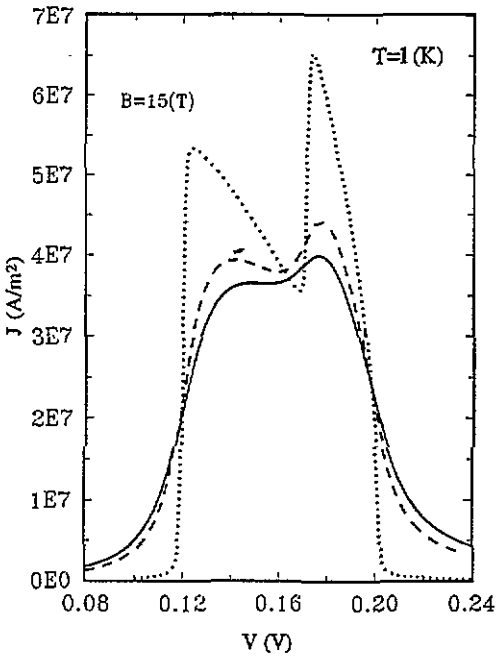

Figure 2. Tunnelling current density J through a DBHS with parameters used in [26]: $b = 50$ Å; $a = 40$ Å; $V_0 = 300$ meV; $m_z^* = 0.067m_0$ and $m_p^* = 0.101m_0$; $\varepsilon_F = 54$ meV; $\varepsilon_0 = 101$ meV; the dotted line is for $\Gamma_i = 0$, the dashed line for $\Gamma_i = 2$ meV and the solid line for $\Gamma_i = 4$ meV.

applied bias is low [28]. Hence, the quasibound level in the well decreases linearly with the applied bias

$$\varepsilon_0' = \varepsilon_0 - \tfrac{1}{2}ev \tag{1}$$

where ε_0' and ε_0 represent, respectively, the quasibound level in the well along the z direction with and without the applied bias.

It is known that, in the STM, the density of the quasibound states in the well is characterized by the following function [18, 29]:

$$\rho_w(\varepsilon_{wz}) = \frac{\Gamma/\pi}{(\varepsilon_{wz} - \varepsilon_r)^2 + \Gamma^2} \tag{2}$$

where Γ is the broadening half-width of the quasibound level. When the inelastic events are present we have $\Gamma = \Gamma_e + \Gamma_i$, where Γ_e can be obtained numerically or analytically if the bias dependence is neglected [30], while Γ_i is treated as a free parameter in the present work. It should be mentioned that the density of the quasibound states is in principle sensitive to the frequency of incoherent events. When the inelastic half-width is too large, the density of the quasibound states used above becomes inadequate [29]. Fortunately, in the magnetoresonant tunnelling experiments, our interest is restricted to $\Gamma \leqslant \hbar\omega$ where ω is the cyclotron frequency.

The applied magnetic field B quantizes the motion of the electrons in the x–y plane (perpendicular to the tunnelling directon), resulting in Landau levels with energies $\varepsilon_{xy} = (n + \frac{1}{2})\hbar\omega$, where n is the level index ($n = 0, 1, 2, \ldots$), $\omega = eB/m_a^*$ (m_a^* is the effective mass of an electron in the electrodes or in the well). We introduce notations $N_l = (n_l, k_{lz})$, $N_w = (n_w, k_{wz})$ and $N_r = (n_r, k_{rz})$ respectively describing the electron states in the emitter, in the well and in the collector. Denoting the electron energies in the emitter by ε_l, in the well by ε_w and in the collector by ε_r, we have the following relations:

$$\varepsilon_l = (\tfrac{1}{2} + n_l)\hbar\omega + \varepsilon_{lz} \tag{3}$$

$$k_{lz} = \frac{(2m_a^*\varepsilon_{lz})^{1/2}}{\hbar} \tag{4}$$

$$\varepsilon_w = (\tfrac{1}{2} + n_w)\hbar\omega + \varepsilon_{wz} \tag{5}$$

$$k_{wz} = \frac{[2m_a^*(\varepsilon_{wz} + \frac{1}{2}ev)]^{1/2}}{\hbar} \tag{6}$$

$$\varepsilon_r = (\tfrac{1}{2} + n_r)\hbar\omega + \varepsilon_{rz} \tag{7}$$

$$k_{rz} = \frac{[2m_a^*(\varepsilon_{rz} + ev)]^{1/2}}{\hbar}. \tag{8}$$

It is worthwhile to point out that from the viewpoint of the STM [11, 17, 18, 29], the electron state density along the z direction in the emitter or collector electrode is determined by the dispersion relation (4) or (8), whereas the density of states in the well is determined by the equation (2) which implicitly takes into account the effects of confinement of the barriers as well as interaction with the continuum outside the well.

The transition rates of an electron from the electrode to the well W_{lw} ($= W_{wl}$) and from the well to the collector electrode W_{wr} ($= W_{rw}$) are respectively

$$W_{lw} = \frac{2\pi}{\hbar}|M_{lw}|^2\delta(\varepsilon_l - \varepsilon_w)\delta(n_l - n_w) \tag{9}$$

$$W_{wr} = \frac{2\pi}{\hbar}|M_{wr}|^2\delta(\varepsilon_w - \varepsilon_r)\delta(n_w - n_r) \tag{10}$$

where M is the Oppenheimer transition Hamiltonian [31, 17, 18]

$$|M_{lw}|^2 = \frac{\hbar^2}{2mLa}[\varepsilon_{lz}(\varepsilon_{lz} + \tfrac{1}{2}ev)]^{1/2}T_l(\varepsilon_{lz}) \tag{11}$$

$$|M_{wr}|^2 = \frac{\hbar^2}{2mLa}[(\varepsilon_{wz} + \tfrac{1}{2}ev)(\varepsilon_{wz} + ev)]^{1/2}T_r(\varepsilon_{wz}) \tag{12}$$

where a is the width of the well, L is the width of the emitter or collector, T_l and T_r are respectively the transmission coefficients that electrons tunnel through the left barrier and right barrier. Under the step potential approximation (shown in figure 1(b)), by using the transfer-matrix technique T_l and T_r can be expressed as

$$T_l = \begin{cases} \dfrac{4k_{wz}/k_{lz}}{(1+k_{wz}/k_{lz})^2\cosh^2(k_{b1}b)+(k_{wz}/\gamma k_{b1}-\gamma k_{b1}/k_{lz})^2\sinh^2(k_{b1}b)} & \text{if } V_0 - \frac{b}{2b+a}\frac{ev}{2} - \varepsilon_{lz} > 0 \\ \dfrac{4k_{wz}/k_{lz}}{(1+k_{wz}/k_{lz})^2+(k_{wz}b/\gamma)^2} & \text{if } V_0 - \frac{b}{2b+a}\frac{ev}{2} - \varepsilon_{lz} = 0 \\ \dfrac{4k_{wz}/k_{lz}}{(1+k_{wz}/k_{lz})^2\cos^2(k'_{b1}b)+(k_{wz}/\gamma k'_{b1}-\gamma k'_{b1}/k_{lz})^2\sin^2(k'_{b1}b)} & \text{if } V_0 - \frac{b}{2b+a}\frac{ev}{2} - \varepsilon_{lz} < 0 \end{cases} \tag{13}$$

and

$$T_r = \begin{cases} \dfrac{4k_{rz}/k_{wz}}{(1+k_{rz}/k_{wz})^2\cosh^2(k_{b2}b)+(k_{rz}/\gamma k_{b2}-\gamma k_{b2}/k_{wz})^2\sinh^2(k_{b2}b)} & \text{if } V_0 - \frac{3b+2a}{2b+a}\frac{ev}{2} - \varepsilon_{wz} > 0 \\ \dfrac{4k_{rz}/k_{wz}}{(1+k_{rz}/k_{wz})^2+(k_{rz}b/\gamma)^2} & \text{if } V_0 - \frac{3b+2a}{2b+a}\frac{ev}{2} - \varepsilon_{wz} = 0 \\ \dfrac{4k_{rz}/k_{wz}}{(1+k_{rz}/k_{wz})^2\cos^2(k'_{b2}b)+(k_{rz}/\gamma k'_{b2}-\gamma k'_{b2}/k_{wz})^2\sin^2(k'_{b2}b)} & \text{if } V_0 - \frac{3b+2a}{2b+a}\frac{ev}{2} - \varepsilon_{wz} < 0 \end{cases} \tag{14}$$

where b and V_0 are respectively the barrier width and the height, $\gamma = m_a^*/m_b^*$ (m_b^* is the effective mass of an electron in the barriers) and the wavevectors in the barriers are determined from the parabolic energy–momentum relation

$$k_{b1} = \left[2m_b^*\left(V_0 - \frac{b}{2a+b}\frac{ev}{2} - \varepsilon_{1z}\right)\right]^{1/2}\Big/\hbar \tag{15}$$

$$k'_{b1} = \left[2m_b^*\left(-V_0 + \frac{b}{2a+b}\frac{ev}{2} + \varepsilon_{1z}\right)\right]^{1/2}\Big/\hbar \tag{16}$$

$$k_{b2} = \left[2m_b^*\left(V_0 - \frac{3b+2a}{2a+b}\frac{ev}{2} + \varepsilon_{wz}\right)\right]^{1/2}\Big/\hbar \tag{17}$$

$$k'_{b2} = \left[2m_b^*\left(-V_0 + \frac{3b+2a}{2a+b}\frac{ev}{2} + \varepsilon_{wz}\right)\right]^{1/2}\Big/\hbar. \tag{18}$$

The current density of the system is given by the following equation:

$$\begin{aligned} J &= e\sum_{N_1,N_w}\{W_{1w}f_1(\varepsilon_1)[1-f_w(\varepsilon_w)] - W_{w1}f_w(\varepsilon_w)[1-f_1(\varepsilon_1)]\} \\ &= e\sum_{N_1}\frac{2\pi}{\hbar}|M_{1w}|^2[f_1(\varepsilon_1)-f_w(\varepsilon_1)]\rho_w(\varepsilon_{1z}) \\ &= e\omega\frac{(2m_a^*)^{1/2}}{4\pi a\hbar}\sum_{N_1}\int_0^\infty(\varepsilon_{1z}+\tfrac{1}{2}ev)^{1/2}T_1(\varepsilon_z)[f_1(\varepsilon_1)-f_w(\varepsilon_1)]\rho_w(\varepsilon_{1z})\,d\varepsilon_{1z} \end{aligned} \tag{19}$$

where f_1 and f_w are the electron distribution functions respectively in the emitter and the well. When there exists a steady current, f_w is determined by the balancing equation

$$\frac{df_w}{dt} = \sum_{N_1}W_{1w}[f_1(\varepsilon_1)-f_w(\varepsilon_w)] - \sum_{N_r}W_{wr}[f_w(\varepsilon_w)-f_r(\varepsilon_r)] = 0 \tag{20}$$

where f_r is the distribution function in the collector. Assuming that the distribution function of electrons in the emitter and in the collector satisfy the Fermi–Dirac distribution ($f_1(\varepsilon_1) = \{\exp[(\varepsilon_1-\varepsilon_F)/KT]+1\}^{-1}$, $f_r(\varepsilon_r) = \{\exp[(\varepsilon_r+ev-\varepsilon_F)/KT]+1\}^{-1}$), the steady-state distribution function in the well is found to be

$$f_w = \frac{T_1(\varepsilon_{wz})f_1(\varepsilon_w)+T_r(\varepsilon_{wz})f_r(\varepsilon_w)}{T_1(\varepsilon_{wz})+T_r(\varepsilon_{wz})}. \tag{21}$$

Combining equations (19) and (21) the current density is finally given by

$$J = \frac{e\omega}{4\pi a}\frac{(2m_a^*)^{1/2}}{\hbar}\sum_{n_1}\int_0^\infty(\varepsilon_{1z}+\tfrac{1}{2}ev)^{1/2}\frac{T_1(\varepsilon_{1z})T_r(\varepsilon_{1z})}{T_1(\varepsilon_{1z})+T_r(\varepsilon_{1z})}[f_1(\varepsilon_1)-f_r(\varepsilon_1)]\rho_w(\varepsilon_{1z})\,d\varepsilon_{1z} \tag{22}$$

from which the differential conductance per unit area $\sigma = \partial J/\partial v$ can also be calculated.

It is known that space-charge accumulation in the electrodes and in the well bend the bottom of the conduction band near the interfaces. In order to include this effect, we assume that the space-charge distribution in the electrodes and in the well is homogeneous. The area charge densities in the electrodes are evaluated by the method given in [20], while the area charge density in the well can be obtained from equation (21). By applying the Gauss law, the step potential approximation of DBHSs can be given as follows:

$$V(z) = \begin{cases} 0 & \text{if } z < 0 \\ e\frac{\delta_e\sigma_e}{8\varepsilon} & \text{if } 0 \leqslant z < \delta_e \\ V_0 + e\frac{(\delta_e+b)\sigma_e}{2\varepsilon} & \text{if } \delta_e \leqslant z \leqslant \delta_e + b \\ e\frac{(\delta_e+a+2b)\sigma_e}{2\varepsilon} + e\frac{a\sigma_w}{8\varepsilon} & \text{if } \delta_e + b < z < \delta_e + b + a \\ V_0 + e\frac{(\delta_e+2a+3b)\sigma_e}{2\varepsilon} + e\frac{(a+b)\sigma_w}{2\varepsilon} & \text{if } \delta_e + b + a \leqslant z \leqslant \delta_e + 2b + a \\ e\frac{(\delta_e+a+2b+0.75\delta_c)\sigma_e}{2\varepsilon} + e\frac{(a+2b+0.75\delta_c)\sigma_w}{2\varepsilon} & \text{if } \delta_e + 2b + a < z \leqslant \delta_e + 2b + a + \delta_c \\ -ev & \text{if } z > \delta_e + 2b + a + \delta_c \end{cases} \tag{23}$$

where ε is the static dielectric constant; δ_e or δ_c is the width of the space-charge accumulation layer in the emitter or collector

$$\delta_e = e^{-1}\left[\frac{2\varepsilon}{N(\varepsilon_F)}\right]^{1/2} \tag{24}$$

and

$$\delta_c = \left[\frac{\lambda}{\varepsilon(\delta_e + a + 2b)^{-1}v - 0.5\sigma_w}\right]^{1/5}. \tag{25}$$

In equation (24) $N(\varepsilon_F)$ is the density of states at the Fermi energy; in equation (25)

$$\lambda = \frac{36\pi^4}{e^2}\left(\frac{\varepsilon\hbar^2}{em_a^*}\right)^3 \tag{26}$$

σ_w is the area charge density in the well

$$\sigma_w = -\frac{em_a^*\omega}{\pi\hbar}\sum_{n_1}\int_0^\infty \frac{T_l(\varepsilon_{lz})f_l(\varepsilon_l) + T_r(\varepsilon_{lz})f_r(\varepsilon_l)}{T_l(\varepsilon_{lz}) + T_r(\varepsilon_{lz})}\rho_w(\varepsilon_{lz})\,d\varepsilon_{lz} \tag{27}$$

σ_e is the area charge density of the accumulation layer in the emitter

$$\sigma_e = -2\varepsilon\frac{v}{\delta_e + 2a + 4b + \delta_c} - \frac{a + 2b + \delta_c}{\delta_e + 2a + 4b + \delta_c}\sigma_w. \tag{28}$$

According to equation (23), equation (1) should be modified as

$$\varepsilon_0' = \varepsilon_0 + e(\delta_e + a + 2b)\frac{\sigma_e}{2\varepsilon} + ea\frac{\sigma_w}{8\varepsilon}. \tag{29}$$

Combining with equations (23) and (27)–(29), T_l and T_r can be calculated self-consistently by means of the transfer-matrix technique considering the space-charge formation in the electrodes and well. So the tunnelling current density and the differential conductance can be obtained from equation (22) again.

3. Results and discussion

For comparison with theoretical calculations of the previous works [26] based upon the GTM through the whole structure, we calculate the current densities with the same parameters without considering the effects of the space-charge formation in the electrodes and well. The results for current density calculated here (shown in figure 2) are the same as their numerical calculations (figure 2 in [26]) in the overall shape and peak positions as well as the order of magnitude. But our results display the tendency that the magnitudes of the current density curves decrease gradually with increasing inelastic-scattering half-width, in accordance with the prediction of [29]. Therefore it may be concluded that equivalence between the STM and the GTM is preserved when a magnetic field is applied and inelastic-scattering broadening is included. At $\Gamma_i = 0$, the equivalence between the STM and the GTM has been discussed in [18]. The resemblance to previous work is not surprising since [29] has shown that the state density of equation (2) is valid in the crossover from elastic scattering to inelastic scattering. It is worthwhile to point out that the GTM requires a calculation of the total transmission coefficient while the STM requires a calculation of the transmission coefficients of single barriers. Numerical results between the two methods may differ a little. When Γ_i is so large that the density of states cannot be written in the form of equation (2), the two methods are no longer equivalent.

As a matter of fact, the quasibound-level broadening Γ ($\sim$ meV) in the well is much smaller than the ground-state energy ε_0 ($\sim$ 100 meV) for DBHSs with a well of 40 Å or wider. One also knows that in the resonant region both $T_l(\varepsilon_0')$ and $T_r(\varepsilon_0')$ are slowly varying functions of the applied bias and therefore may be approximately regarded as insensitive to the applied bias [28]. When the temperature is low enough, the Fermi–Dirac distribution function takes the form of a step function when quasi-Fermi energy is introduced taking into account the thermal equilibrium with the nearby contacts. That is to say that we can set $f_r = 0$ (in the resonant region $ev \gg \varepsilon_F$) for the collector, whereas $f_l = 1$ ($\varepsilon_l \leqslant \varepsilon_F$) or $f_l = 0$ ($\varepsilon_l > \varepsilon_F$) for the emitter. Then equation (22) is rewritten as

$$J = \frac{e\omega(2m_a^*\varepsilon_0)^{1/2}}{4\pi a\hbar}\frac{T_l(\varepsilon_0')T_r(\varepsilon_0')}{T_l(\varepsilon_0')+T_r(\varepsilon_0')}\sum_{n_l=0}^{N}\int_0^{\varepsilon_n}\frac{\Gamma/\pi}{(\varepsilon_{lz}-\varepsilon_0')^2+\Gamma^2}\,\mathrm{d}\varepsilon_{lz} \tag{30}$$

where $\varepsilon_n = \varepsilon_F - (\frac{1}{2}+n_l)\hbar\omega$. After integration over ε_{lz} we finally obtain

$$J = \frac{e\omega(2m_a^*\varepsilon_0)^{1/2}}{4\pi a\hbar}\frac{T_l(\varepsilon_0')T_r(\varepsilon_0')}{T_l(\varepsilon_0')+T_r(\varepsilon_0')}\sum_{n_l=0}^{N}\left(\tan^{-1}\frac{\varepsilon_n-\varepsilon_0'}{\Gamma}+\tan^{-1}\frac{\varepsilon_0'}{\Gamma}\right) \tag{31}$$

where N is an integer satisfying

$$\varepsilon_F - (\tfrac{1}{2}+N)\hbar\omega > 0. \tag{32}$$

The differential conductance is consequently determined by

$$\sigma = \frac{e^2\omega(2m_a^*\varepsilon_0)^{1/2}}{8\pi a\hbar}\frac{T_l(\varepsilon_0')T_r(\varepsilon_0')}{T_l(\varepsilon_0')+T_r(\varepsilon_0')}\sum_{n_l=0}^{N}\left[\frac{\Gamma}{(\varepsilon_n-\varepsilon_0')^2+\Gamma^2}-\frac{\Gamma}{(\varepsilon_0')^2+\Gamma^2}\right]. \tag{33}$$

Provided that $\varepsilon_0' \gg \Gamma$ in the resonant region, we have approximately

$$\sigma = \frac{e^2\omega(2m_a^*\varepsilon_0)^{1/2}}{8\pi a\hbar}\frac{T_l(\varepsilon_0')T_r(\varepsilon_0')}{T_l(\varepsilon_0')+T_r(\varepsilon_0')}\sum_{n_l=0}^{N}\frac{\Gamma}{[(\varepsilon_F-(\frac{1}{2}+n_l)\hbar\omega-\varepsilon_0']^2+\Gamma^2}. \tag{34}$$

It can be seen that the differential conductance shows oscillation as the applied bias varies and reaches a maximum when

$$\varepsilon_F - \varepsilon_0' - (\tfrac{1}{2} + n_1)\hbar\omega = 0. \tag{35}$$

From equation (33), we can see that the minimum of the negative differential conductance occurs when

$$\varepsilon_0' = 0. \tag{36}$$

Equations (35) and (36) analytically reproduce the main features obtained in the experimental work of Mendez *et al* [19], when combined with equation (32). This is not a surprise since in their analyses the quantum well serves as 'intermediate' resonant states, through which tunnelling takes place, and remains unoccupied otherwise. These ideas are in fact the same as those in the sequential tunnelling model of Luryi. Besides the quantitative agreement discussed above, one virtue of the present results, equations (31) and (34), is that simple expressions for the resonant current and the oscillatory differential conductance are derived which could be used to compare with experiments quantitatively. Other theoretical works [21, 22], based upon the total transmission coefficient of the whole structure, are in general not so straightforward and need much more numerical calculation.

In order to quantitatively compare with the experimental results in [21], we have performed numerical calculations of the current density and differential conductance for a DBHS starting from the expression of equation (22) at $\Gamma < \hbar\omega$. The DBHS consists of a GaAs well of width 40 Å sandwiched between two $Ga_{1-x}Al_xAs$ barriers of width 100 Å, where $x = 0.33$ corresponds to a barrier height of 0.3 eV. The two electrodes are assumed to be doped uniformly to a level of electron concentration of 7×10^{23} m^{-3} yielding a Fermi energy of about 0.43 eV. The effective masses are chosen to be $0.067m_0$ and $0.101m_0$, respectively, in the well and barrier regions, where m_0 is the free electron mass. We find the ground state in the well is $\varepsilon_0 = 0.118$ eV when no bias is applied [30]. We firstly perform the numerical calculation at $\Gamma_i = 5$ meV without considering the effects of the space-charge formation in the electrodes and well. The results are shown in figure 3. It can be seen that in this case there are considerable quantitative discrepancies between the experimental results and theoretical calculations in both overall shape and peak value positions of J–v and σ–v curves. In particular, there are negative maxima in the σ–v curves when $B = 5$ T and 10 T. We believe that these discrepancies result from our ignoring the space-charge formation in the electrodes and well. Figure 4 shows that the influence of the space-charge formation is remarkable. It can be seen that at $\Gamma_i = 5$ meV the results of figure 4 here are in good agreement with the experimental results of figures 3 and 4 in [21] not only in the overall shape of the curves but also the peak positions. In particular, the position of the negative differential conductance is almost equal to the measured value of experiments (our calculation value, $v \simeq 0.263$ eV; experimental value, $v \simeq 0.27$ eV). Note that the variation of Γ_i changes the overall shape of the curves as well as broadening the resonance but it does not change the positions of the peak and valley values of the curves.

In fact, the influence of the space-charge formation in the electrodes and well can be analytically seen from (29), (35) and (36). From (29) and (35), we obtain the peak positions of the differential conductance

$$ev_{n_1} = \alpha^{-1}(\varepsilon_0 - \varepsilon_F - \Delta) + \alpha^{-1}(\tfrac{1}{2} + n_1)\hbar\omega \tag{37}$$

with

$$\alpha = \frac{\delta_e + a + 2b}{\delta_e + 2a + 2b + \delta_c} \tag{38}$$

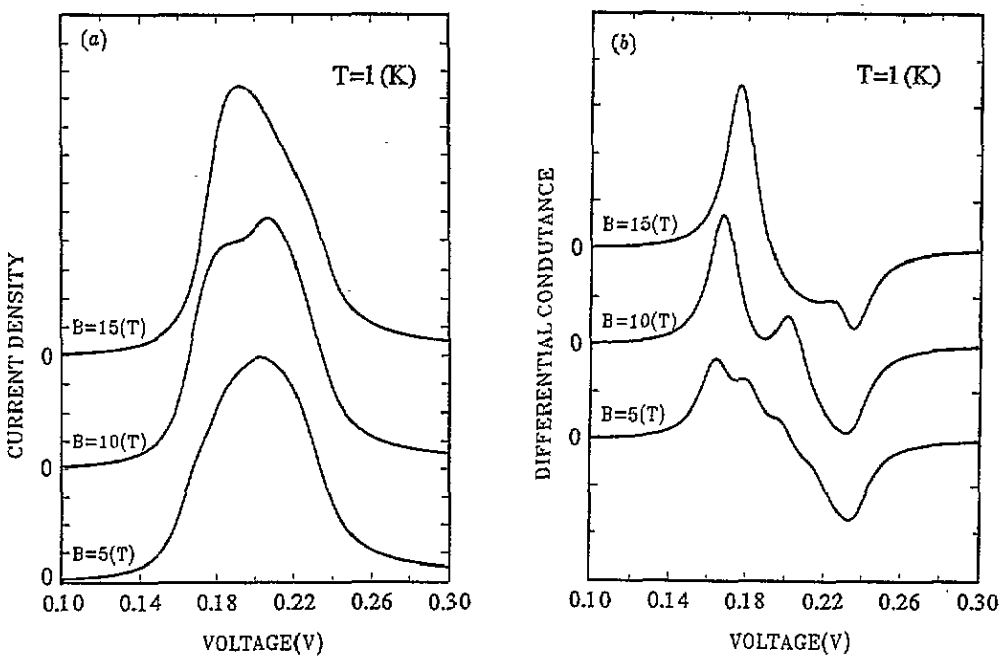

Figure 3. (*a*) Current density J as a function of applied voltage for the DBHS with parameters stated in the text, without considering the space-charge formation in the electrodes and well. (*b*) Differential conductance σ as a function of applied voltage under the same conditions as (*a*). For clarity, the J–v and σ–v curves have been offset by a value of 6×10^3 A m^{-2} and 4×10^5 Ω^{-1} m^{-2} for neighbouring magnetic fields, respectively.

and

$$\Delta = e\left[\frac{(\delta_e + a + 2b)(a + 2b + \delta_c)}{\delta_e + 2a + 4b + \delta_c} - \frac{a}{4}\right]\frac{\sigma_w}{\varepsilon}. \tag{39}$$

From (29) and (36), we find that the negative differential conductance occurs at

$$ev_- = \alpha^{-1}(\varepsilon_0 - \Delta). \tag{40}$$

In the resonant region, we find that δ_c and σ_w are insensitive to the applied bias v. For the DBHS with $a = 40$ Å and $b = 100$ Å, we have $\alpha \simeq 0.46$, $\sigma_w \simeq 0.7 \times 10^{-4}$ C m^{-2} and $\Delta \simeq -3$ meV yielding $v_- \simeq 0.263$ V. If ignoring the effects of the space-charge formation in the electrodes and well, we have $\delta_e = \delta_c = 0$ and $\sigma_w = 0$ yielding $v_- = 0.236$ V. The analytical results again show that the effects of the space-charge formation in the electrodes and well are significant.

From equation (37), we can see that for a given applied bias the resonant peak may occur many times with increasing B when $n_l > 1$ satisfying equation (37). The oscillatory behaviour is periodic in $1/B$, with the period

$$T_p = \frac{e\hbar}{m_d^*(\varepsilon_F - \varepsilon_0 + \alpha e v + \Delta)}. \tag{41}$$

This kind of periodic oscillatory behaviour can be clearly seen from the J–B curves shown in figure 5.

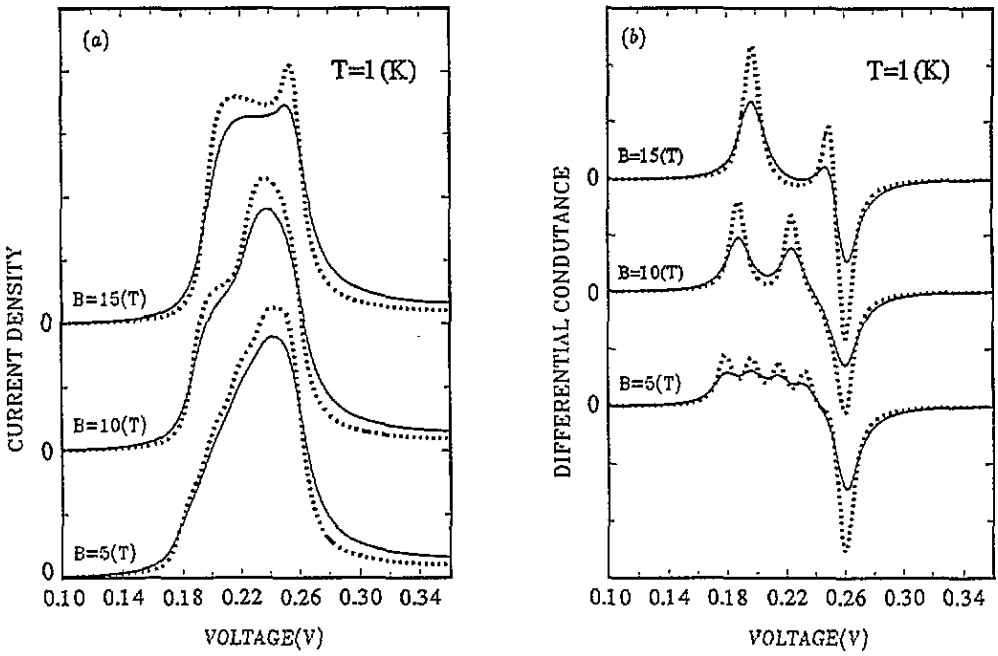

Figure 4. (*a*) J–v characteristics for the same structure as figure 3, with the space-charge formation in the electrodes and well considered. (*b*) σ–v characteristics under the same conditions as (*a*). For clarity, the J–v and σ–v curves have been offset by a value of 2×10^4 A m^{-2} and 2×10^6 Ω^{-1} m^{-2} for neighbouring magnetic fields, respectively. The dotted line is for $\Gamma_i = 3$ meV, the solid line for $\Gamma_i = 5$ meV.

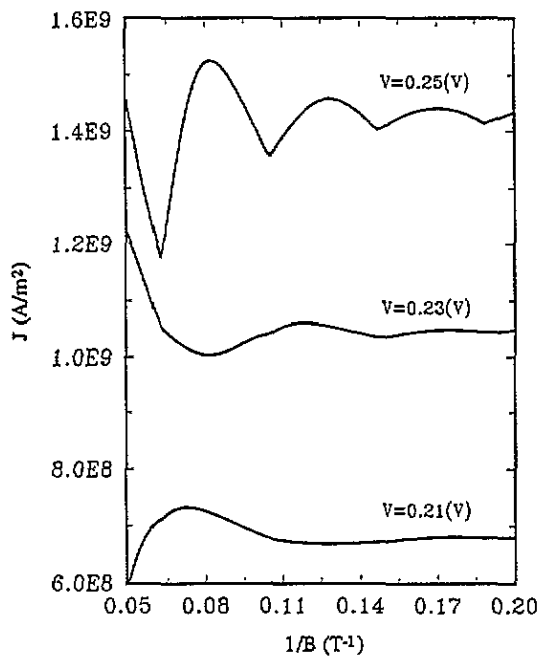

Figure 5. J–B characteristics at different fixed biases for the structure of figure 4 with a different barrier width of $b = 30$ Å. A value of $\Gamma_i = 0$ meV is assumed. The effects of the space-charge formation in the electrodes and well are taken into account.

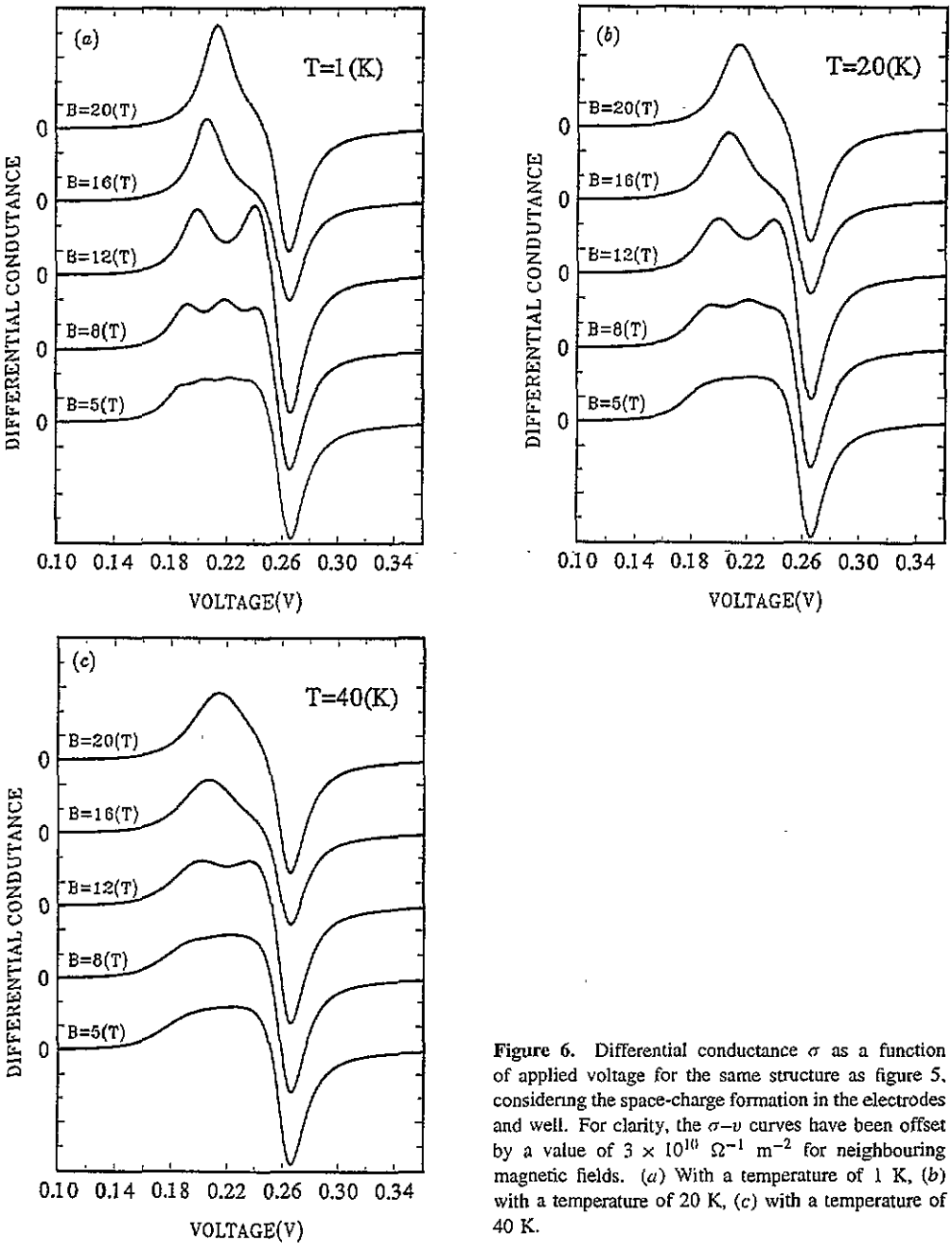

Figure 6. Differential conductance σ as a function of applied voltage for the same structure as figure 5, considering the space-charge formation in the electrodes and well. For clarity, the σ–v curves have been offset by a value of 3×10^{10} Ω^{-1} m^{-2} for neighbouring magnetic fields. (*a*) With a temperature of 1 K, (*b*) with a temperature of 20 K, (*c*) with a temperature of 40 K.

In order to study the temperature dependence of resonant tunnelling in detail, we plot the σ–v curves for magnetic fields ranging from 5 T to 20 T at temperatures 1 K, 20 K and 40 K respectively in figures 6(*a*), 6(*b*) and 6(*c*), considering the effects of space-charge formation in the electrodes and well. For clarity the current-density curves are offset by a value of 3×10^8 A m^{-2} for neighbouring magnetic fields. Our calculations show that the modulations induced by Landau levels in the differential conductance curves are well

resolved at low temperature. For magnetic fields of 5, 8 and 12 T there are respectively four, three and two peaks observed in accordance with equation (32). For magnetic fields $B > 16$ T, the quantum limit is reached and thus only the lowest Landau level is occupied. The tendency is observed that modulation arising from the Landau levels is smeared and the shapes of the curves tend to the limit of $B = 0$ as the temperature is increased. This confirms that the Landau level splitting must be large compared to the thermal energy. This can be seen in figure 4(*b*) where the oscillations at a magnetic field of 5 T vanish, while those at higher magnetic field can still be resolved at a temperature of 20 K.

Acknowledgments

This work was supported by the Chinese Higher Education Foundation and two of us (W S Li and Y Y Yeung) would like to thank the UPGC, Hong Kong, for financial support.

References

[1] Tsu R and Esaki L 1973 *Appl. Phys. Lett.* **22** 562
[2] Chang L L, Esaki L and Tsu R 1974 *Appl. Phys. Lett.* **24** 593
[3] Ricco B and Azbel M Y 1984 *Phys. Rev.* B **29** 1970
[4] Mendez E E, Wang W I, Ricco B and Esaki L 1985 *Appl. Phys. Lett.* **47** 415
[5] Luryi S and Caps F 1985 *Appl. Phys. Lett.* **47** 1347
[6] Capasso F and Kiehl R A 1983 *J. Appl. Phys.* **58** 1366
[7] Luryi S 1985 *Appl. Phys. Lett.* **47** 490
[8] Morkoc H, Chen, Reddy V K, Henderson T and Luryi S 1986 *Appl. Phys. Lett.* **49** 70
[9] Sollner T C L G, Goodhue W D, Tannawald P E, Parker C D and Peck D D 1983 *Appl. Phys. Lett.* **43** 558
[10] Goldman V J, Tsui D C and Cunningham J E 1987 *Phys. Rev. Lett.* **58** 1256
[11] Sheard F W and Toombs G A 1988 *Appl. Phys. Lett.* **52** 1228
[12] Sheard V J and Toombs G A *1992 Semicond. Sci. Technol.* 7 B460
[13] Leadbeater M L, Alves E S, Sheard F W, Eaves L, Henini M, Hughes O H and Toombs G A 1989 *J. Phys.: Condens. Matter* **1** 10605
[14] Pernas P L, Flores F and Anda E V 1993 *Phys. Rev.* B **47** 4779
[15] Vassell M O, Johnson L and Lockwood H F 1983 *J. Appl. Phys.* **54** 5206
[16] Peng J P, Chen H and Zhou S X 1989 *J. Phys.: Condens. Matter* **1** 5451
[17] Payen M C 1986 *J. Phys. C: Solid State Phys.* **19** 1145
[18] Weil T and Vinter B 1987 *Appl. Phys. Lett.* **50** 1281
[19] Mendez E E, Esaki L and Wang W I 1986 *Phys. Rev.* B **33** 2893
[20] Goldman V J, Tsui D C and Cunningham J E *1987 Phys. Rev.* B *35* 9387
[21] Goncalves C E T and Mendez E E 1988 *Phys. Rev.* B **38** 3394
[22] Pötz W 1990 *Phys. Rev.* B **41** 12111
[23] Marigliano R V, Tagliacozzo A, Ventriglia F and Zucchelli G P 1991 *Phys. Rev.* B **43** 2201
[24] Galvao G Y, Berroir J M, Guldner Y and Vieren J P 1991 *Phys. Rev.* B **44** 13795
[25] Kutter C, Chitta V, Maan J C, Fal'ko V I, Leadbeater M L, Henini M and Eaves L 1992 *Phys. Rev.* B **45** 8749
[26] Schulz P A and Tejedor C 1990 *Phys. Rev.* B **41** 3053
[27] Platero G, Brey L and Tejedor C 1989 *Phys. Rev.* B **40** 8548
[28] Zou N Z, Rammer J and Chao K A 1992 *Phys. Rev.* B **46** 15912
[29] Büttiker M 1988 *IBM J. Res. Dev.* **32** 63
[30] Peng J P, Mu Y M and Chen X C 1993 *J. Appl. Phys.* **73** 989
[31] Bardeen J 1961 *Phys. Rev. Lett.* **6** 57